ASIGN: An Anatomy-aware Spatial Imputation Graphic Network for 3D Spatial Transcriptomics

Supplementary Material

1. Dataset Details

1.1. Details in Public Datasets

We employed the HER2 [1], ST-data [3], and DLPFC [4] datasets for cross-validation of our model. The ST-data dataset comprises 23 breast cancer histopathological samples, each consisting of 2 or 3 adjacent layers with a thickness of 16 μm. The HER2 dataset includes 8 samples containing 6 or 3 adjacent layers, while the DLPFC dataset features 3 samples, each composed of 4 directly adjacent 10 μm consecutive tissue sections from the human dorsolateral prefrontal cortex. All whole-slide images (WSIs) were scanned at 10x magnification.

To ensure the accuracy of 3D sample-level information, we excluded 7 samples from the ST-data dataset due to suboptimal registration quality. Figure 1 provides detailed information about each sample used in the three datasets, along with their summarized profiles.

1.2. Multi-resolution Patches and Gene Selection

We extracted patches at multiple resolutions, specifically at the spot level, region level, and global level, by cropping the images to sizes of 224×224, 512×512, and 1024×1024 pixels, respectively. The relationships between patches across different resolution levels were established by analyzing their spatial overlaps, ensuring consistent alignment across scales. Detailed information on the multi-resolution patches, including their distribution and characteristics for each public dataset, is presented in Figure 1.

To determine the ground truth values for the region and global levels, y_r and y_g, we aggregated the spot-level gene expression values within their respective region and global areas. This process is mathematically expressed as:

$$y_r = \sum_{i \in R} y_i, \quad y_g = \sum_{i \in G} y_i \tag{1}$$

Here, y_i denotes the gene expression value at the i-th spot, R represents the set of spots within a specific region, and G denotes the set of spots within the global area. This approach ensures a consistent representation of gene expression across multiple spatial levels.

Following the methodology outlined in ST-Net [3], we selected the top 250 genes with the highest average expression for prediction. Figure 3 provides details of the selected genes and the corresponding codes for each dataset.

2. Implementation Details

2.1. Data Augmentation

To improve the model's generalization ability and ensure consistency across all experiments, we implemented a standardized data augmentation strategy. This approach included random horizontal and vertical flips to simulate variations in image orientation, random 90-degree rotations to enhance rotational invariance, and final normalization to adjust pixel values to align with the standard distribution used by pretrained models (mean [0.485, 0.456, 0.406] and standard deviation [0.229, 0.224, 0.225]).

2.2. 3D Global Alignment

We utilized Xfeat [6] for feature extraction and ANTs [7] for WSI-level image registration. Figure 2 visualizes the 3D global alignment results and the aligned spots for a 6-layer sample. To achieve this, we extracted geometric transformation parameters between images (scaling, rotation, and translation), generated inverse affine matrices for each image relative to the reference image, and combined multiple transformation matrices through matrix multiplication to ensure effective transmission of registration information across different layers.

The middle image was designated as the reference image and left untransformed, serving as the baseline, and directly saved to the reconstruction directory to minimize accumulated computational errors. During the registration process, transformations were applied recursively: forward for images preceding the middle image and backward for those following it, completing a bidirectional registration workflow. To accelerate the process, the symmetric normalization algorithm was employed using 8 threads.

Following the completion of the 3D WSI global alignment, we performed the 3D spot-level alignment. For each spot in the original image, circles with a radius of 112 pixels were drawn, and 100 points were plotted within each circle. Using the transformation matrices derived from the global alignment, these circles were aligned at the spot level to identify cross-layer spot overlap information. This overlap data was subsequently utilized to construct the 3D sample-level graph by establishing connections between spots.

2.3. Implementation Details for Baselines

To ensure a fair and consistent comparison between the baseline methods and our proposed ASIGN framework, we made minimal yet necessary adjustments to the implemen-

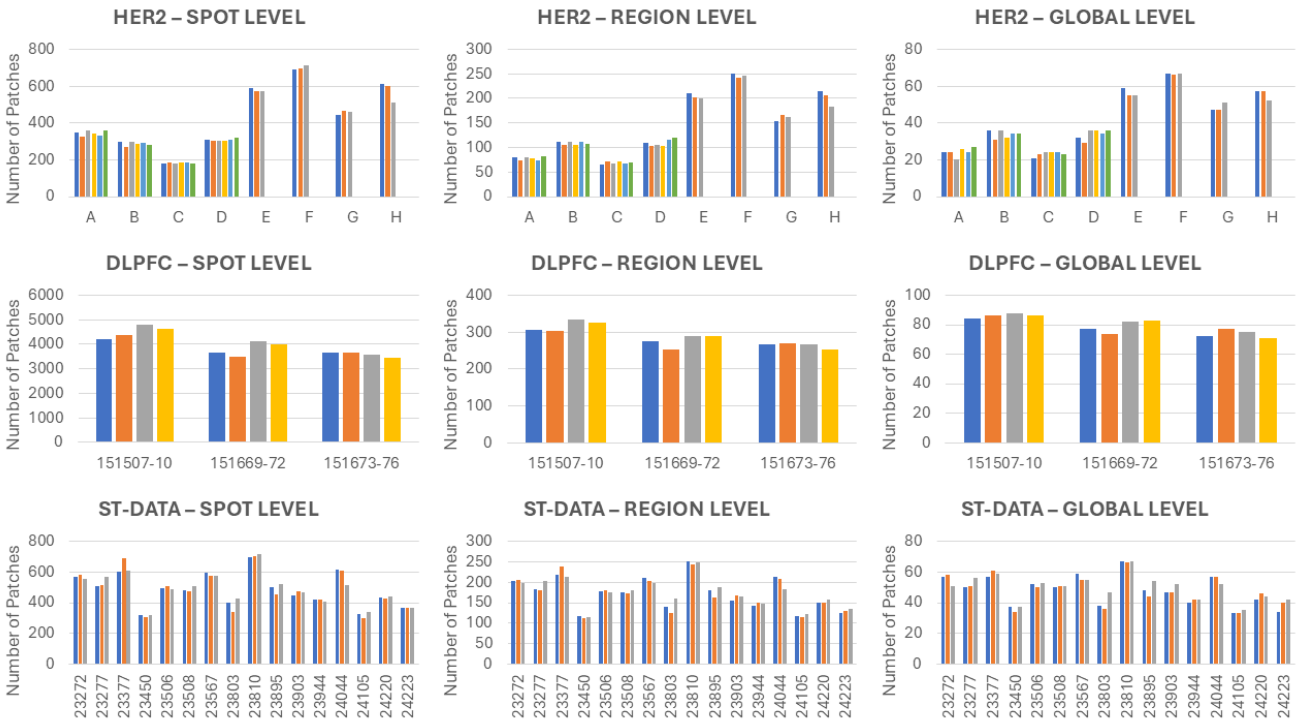

Figure 1. **Profile of public datasets.** This figure provides an overview of the profiles and the distribution of multi-resolution patches extracted from the HER2, DLPFC, and ST-Data datasets across multi-layer sample levels.

tation of certain baseline models. These modifications were carefully designed to align input sizes, feature extraction strategies, and imputation methods across all models, ensuring that performance differences could be attributed solely to the respective methodologies rather than inconsistencies in the experimental setup.

For **HisToGene** [5] and **His2ST** [10], which originally utilize spot images of 112×112 pixels, we resized all images to a fixed size of 224×224 pixels to ensure consistent input dimensions across models.

For **EGN** [9], we replaced the originally used GAN-based encoder with a pretrained ResNet50 as the feature extractor, ensuring a consistent feature extraction strategy across all baseline models. In line with the original EGN implementation, we selected the 8 most similar exemplars for each spot for training.

For **BLEEP** [8], we utilized the CLIP model as the backbone and applied the simple average strategy proposed by BLEEP to compute the mean gene expression values of the top 50 nearest spots, which served as the imputation prediction result.

For the **3D Sample-level Similarity-based Imputation**, we calculated the mean gene expression values of the top 20 nearest spots for each spot. This approach ensured a fair comparison with our proposed ASIGN framework by maintaining the same number of reference spots for imputation.

Additionally, we applied the data augmentation strategy described in the previous section uniformly across all models to ensure consistency in data preprocessing. During training, each model was trained until convergence, which was defined as the point where the loss stabilized and no longer exhibited significant changes over successive iterations.

2.4. Implementation Details for ASIGN

In our implementation of the proposed ASIGN framework, we utilized a pretrained ResNet50 to extract 1024-dimensional features from patches at multiple resolutions. A 3-layer GAT block was employed, with the output of each layer passed through a corresponding transformer layer. The features refined by each transformer layer were then weighted and aggregated to generate the final feature representation, which was subsequently fed into a linear layer to produce the model's prediction.

For each spot, we selected the top 12 nearest spots to establish edges and construct a 2D WSI-level graph. The edge weights were defined as the inverse of the Euclidean distance between the centers of the connected spots.

In 3D partially-known scenarios, we designated the first layer of each sample as the known layer for the experiments. For the label propagation block, we performed 10 iterations

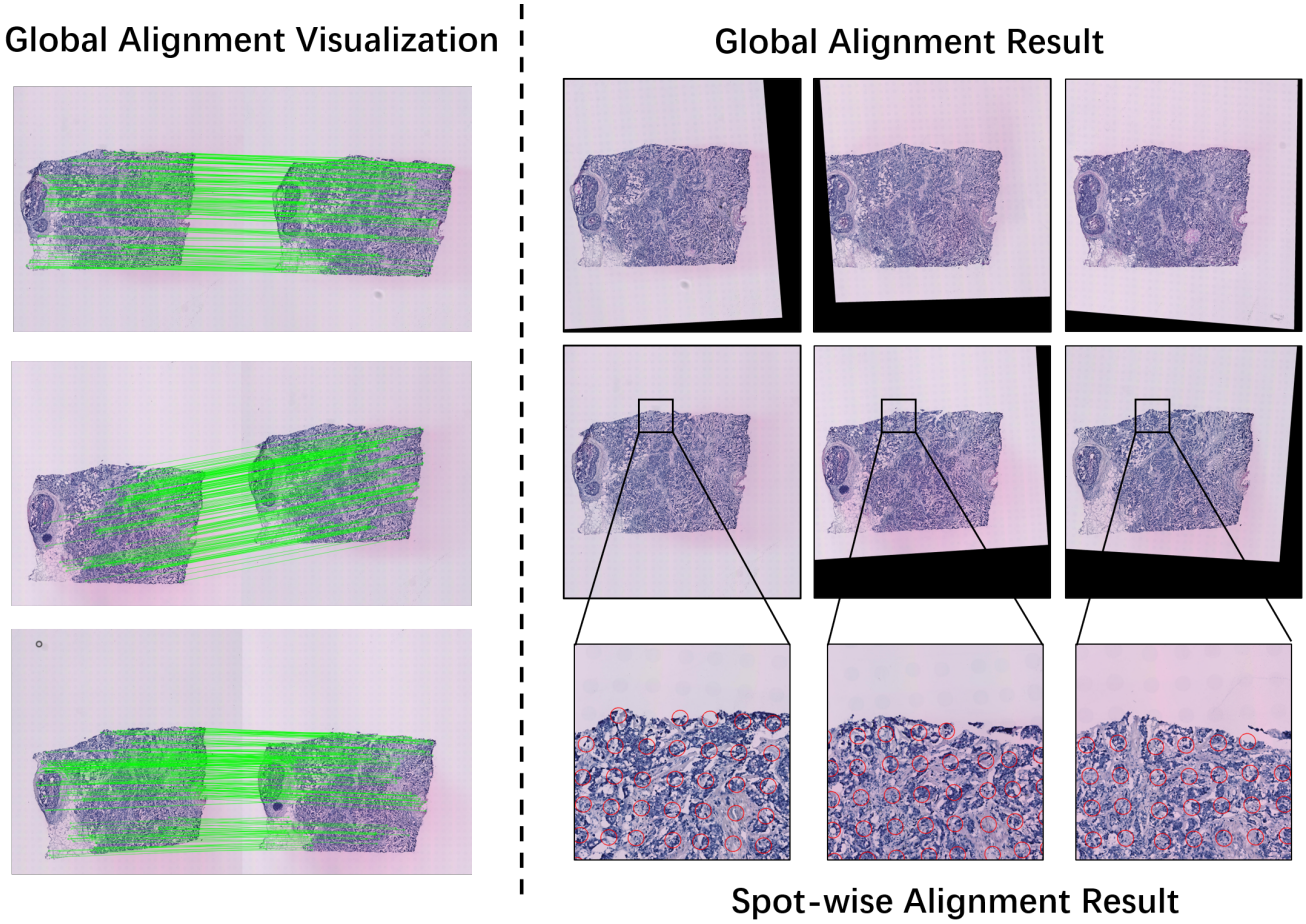

Figure 2. **Visualization of 3D global alignment.** This figure illustrates the 3D global alignment results for a 6-layer sample, showcasing both WSI-level and spot-level alignments. The red circles on the patches represent the spots following 3D global alignment.

to ensure that all unknown nodes were adequately covered while avoiding over-propagation, which could lead to label homogenization and diminish prediction accuracy. Finally, an adaptive weighting mechanism was employed to combine the model's prediction results with the imputation results, producing the final spot-level prediction outputs that effectively leverage both direct predictions and inferred information.

3. Additional Experimental Results

3.1. Computational Costs

ASIGN has **59.45M parameters**. We evaluated computational cost at three scales (batch size = 128) and measured runtime on HER2, summarized in Tab. 1. We iteratively process spot-level subgraphs instead of the entire graph and update only spot-level encoder parameters to minimize computational costs.

Table 1. Computational costs of ASIGN during training.

Patch Size (px)	GPU Memory (GB)	Runtime/epoch (s)	GFLOPs
112x112	7.438	34.76	730.08
224x224	24.68	45.14	2056.61
512x512	113.9	113.89	10617.96

3.2. Analysis of Hyperparameter

A detailed analysis of hyperparameters, including node connection numbers and loss function (shown in Tab. 2) is provided. Increasing inter- and cross-layer connections for each node improves performance until convergence. Consistency constraint loss across multiresolutions enhances predictions, but excessive weights (λ_1, λ_2) introduce additional noise, degrading performance. Proper tuning ensures an optimal balance in optimization.

Table 2. Analysis of hyperparameter tuning.

HER2	Inter-layer	Cross-layer	MSE	MAE	PCC
Connections	4	4	0.479	0.536	0.667
	4	8	0.465	0.526	0.675
	8	16	0.397	0.488	**0.702**
HER2	γ_1	λ_1 & λ_2	MSE	MAE	PCC
Loss Function	0.25	0.75	0.515	0.556	0.654
	0.75	0.25	0.436	0.514	0.671
	1	0	0.46	0.526	0.666
	1	0.5	0.408	0.496	0.696
Ours setting	8 & γ_1=1	12 & λ_1, λ_2=0.25	**0.363**	**0.473**	0.693

3.3. Comparison with TRIPLEX

TRIPLEX [2] is a recently proposed method that effectively utilizes multi-resolution information to generate accurate gene expression predictions. However, due to space constraints, a detailed comparison of TRIPLEX with our proposed ASIGN framework is not included in the main text.

In this section, Table 3 provides a comprehensive comparison of these methods. The experimental results, evaluated across three key metrics, consistently demonstrate the superior performance of our 3D ASIGN framework. By leveraging 3D sample-level information and a cross-layer label imputation strategy, ASIGN achieves significant improvements in all three metrics and outperforms all other baseline methods consistently.

Table 3. Quantitative comparisons between ASIGN and TRIPLEX

Dataset	Model	MSE	MAE	PCC
HER2 [1]	TRIPLEX [2]	0.592	0.591	0.450
	ASIGN 2D	0.579	0.590	0.476
	ASIGN 3D	**0.363**	**0.473**	**0.693**
DLPFC [4]	TRIPLEX [2]	0.645	0.621	0.766
	ASIGN 2D	**0.275**	**0.411**	0.766
	ASIGN 3D	0.353	0.458	**0.773**
ST-Data [3]	TRIPLEX [2]	0.627	0.621	0.553
	ASIGN 2D	0.528	0.566	0.552
	ASIGN 3D	**0.332**	**0.459**	**0.739**

3.4. Additional Ablation Study on Public Datasets

In this section, we provided the experimental results of ablation studies on the ST-Data and DLPFC datasets, which are not included in the main text due to space limitations. These experiments assess the contribution of each functional module in our proposed 3D ASIGN framework and examine the effects of varying known label proportions on gene expression prediction. The results, shown in Table 4 and Table 5, reveal a consistent trend across all datasets, mirroring the findings from the HER2 dataset. This consistency underscores the complementary benefits of each functional block, enabling ASIGN to deliver optimal performance when all modules are integrated.

Table 4. Ablation study on DLPFC Dataset

Ablation Study	MSE	MAE	PCC
w.o GAT & Cross-atten	0.405	0.497	0.767
w.o Cross-atten	0.364	0.470	0.770
w.o GAT	0.368	0.475	0.768
w. Both blocks	**0.353**	**0.458**	**0.773**
w. 0% (w.o CLI)	0.420	0.503	0.770
w. 10%	0.402	0.494	0.772
w. 20% (ASIGN)	0.353	0.458	**0.773**
w. 30%	**0.278**	**0.416**	0.767
2D WSI-wise	**0.275**	**0.411**	0.766
3D Sample-wise	0.420	0.503	**0.770**

Table 5. Ablation study on ST-Data

Ablation Study	MSE	MAE	PCC
w.o GAT & Cross-atten	0.541	0.571	0.706
w.o Cross-atten	0.472	0.535	0.710
w.o GAT	0.451	0.528	0.708
w. Both blocks	**0.332**	**0.459**	**0.739**
w. 0% (w.o CLI)	0.485	0.545	0.604
w. 10%	0.406	0.499	0.708
w. 20% (ASIGN)	0.332	0.459	0.739
w. 30%	**0.329**	**0.458**	**0.741**
2D WSI-wise	0.528	0.566	0.552
3D Sample-wise	**0.485**	**0.545**	**0.604**

References

[1] Alma Andersson, Ludvig Larsson, Linnea Stenbeck, Fredrik Salmén, Anna Ehinger, Sunny Z Wu, Ghamdan Al-Eryani, Daniel Roden, Alex Swarbrick, Åke Borg, et al. Spatial deconvolution of her2-positive breast cancer delineates tumor-associated cell type interactions. *Nature communications*, 12 (1):6012, 2021. 1, 4

[2] Youngmin Chung, Ji Hun Ha, Kyeong Chan Im, and Joo Sang Lee. Accurate spatial gene expression prediction by integrating multi-resolution features. In *Proceedings of the IEEE/CVF Conference on Computer Vision and Pattern Recognition*, pages 11591–11600, 2024. 4

[3] Bryan He, Ludvig Bergenstråhle, Linnea Stenbeck, Abubakar Abid, Alma Andersson, Åke Borg, Jonas Maaskola, Joakim Lundeberg, and James Zou. Integrating spatial gene expression and breast tumour morphology via deep learning. *Nature biomedical engineering*, 4(8): 827–834, 2020. 1, 4

Dataset	Genes to be predicted
HER2	IGKC, TMSB10, ERBB2, IGLC2, IGHG3, IGHA1, GAPDH, ACTB, PSMB3, ACTG1, MUCL1, SERF2, IGHM, PFN1, IGLC3, MIEN1, RACK1, CISD3, CALR, KRT19, TPT1, APOE, FTL, PSAP, SSR4, PTPRF, CTSD, FTH1, FN1, BEST1, FAU, COL1A1, P4HB, UBA52, HLA-B, B2M, EEF2, CD74, FASN, MGP, COL1A2, PSMD3, TFF3, S100A6, MYL6, DDX5, PHB, CFL1, CALML5, SYNGR2, CD63, HLA-C, STARD3, PABPC1, GNAS, TAGLN2, HLA-A, PCGF2, CRIP2, GPX4, GRB7, SLC9A3R1, KRT7, NDUFB9, OAZ1, COL3A1, AEBP1, GNB2, IGHG1, HLA-E, PTMS, FLNA, EIF4G1, PRDX1, SLC25A6, GRINA, AP000769.1, LMNA, CST3, EDF1, ATP5E, EEF1D, ATP6V0B, TUBA1B, MLLT6, HLA-DRA, IGHG4, PPP1R1B, TAGLN, PPP1CA, KRT18, PLXNB2, PRRC2A, KRT81, S100A11, AES, SDC1, SPDEF, S100A9, BGN, CD24, MDK, XBP1, LAPTM5, PLD3, SCAND1, ALDOA, AZGP1, CD81, MMP14, PPDPF, SEC61A1, MZT2B, MIDN, ATP1A1, ADAM15, LASP1, VIM, IFI27, C3, CLDN3, TSPO, APOC1, SPINT2, HNRNPA2B1, PFDN5, EIF4G2, H2AFJ, PRSS8, SPARC, ACTN4, TRAF4, TUBB, S100A14, SCD, SH3BGRL3, COL6A2, ZYX, CYBA, BSG, CTSB, TAPBP, MUC1, TIMP1, CHCHD2, HSP90AB1, CD99, HSPB1, COX6B1, ENO1, UBE2M, MYL9, VMP1, GUK1, H1FX, COX7C, CCT3, C1QA, ATG10, SEPW1, PERP, UBC, RALY, COPE, COX4I1, COX6C, LMAN2, IDH2, HSP90AA1, LGALS1, ORMDL3, INTS1, LAPTM4A, LY6E, COL18A1, CLDN4, MAPKAPK2, NUPR1, CIB1, UQCRQ, SSR2, KDELR1, ARHGDIA, MMACHC, LGALS3, BST2, A2M, CHPF, JUP, POSTN, HSPA8, COPS9, C12orf57, MYH9, GNAI2, COMP, ELOVL1, CALM2, STARD10, PGAP3, NBL1, PEBP1, NDUFB7, ATP5B, KIAA0100, TCEB2, COX5B, SNRPB, HSP90B1, PSMB4, UQCR11, PIP4K2B, PTBP1, ATP5G2, GRN, JTB, PTMA, NUCKS1, IGFBP2, RABAC1, LSM4, LUM, NDUFA3, NACA, FKBP2, RRBP1, ROMO1, SLC2A4RG, TXNIP, ERGIC1, VCP, PCSK7, LGALS3BP, HM13, H3F3B, DHCR24, PFKL, EIF3B, COX8A, PCBP2, C4orf48, ISG15, PNMT, FNBP1L, KDELR2, UBL5, MAP3K12, RHOC, PSMD8, NDUFA11
DLPFC	ENSG00000198804, ENSG00000198712, ENSG00000198938, ENSG00000198886, ENSG00000198899, ENSG00000198888, ENSG00000198763, ENSG00000198727, ENSG00000198840, ENSG00000167996, ENSG00000087250, ENSG00000101439, ENSG00000034510, ENSG00000229117, ENSG00000111640, ENSG00000132639, ENSG00000198786, ENSG00000154146, ENSG00000120885, ENSG00000075624, ENSG00000197971, ENSG00000123416, ENSG00000198668, ENSG00000189043, ENSG00000143933, ENSG00000269028, ENSG00000087460, ENSG00000166165, ENSG00000205542, ENSG00000255823, ENSG00000110484, ENSG00000156508, ENSG00000164919, ENSG00000163032, ENSG00000137818, ENSG00000187094, ENSG00000178980, ENSG00000109475, ENSG00000152583, ENSG00000087086, ENSG00000154277, ENSG00000128245, ENSG00000196262, ENSG00000130558, ENSG00000111775, ENSG00000136156, ENSG00000170315, ENSG00000133318, ENSG00000139970, ENSG00000197756, ENSG00000131143, ENSG00000080824, ENSG00000123560, ENSG00000144713, ENSG00000096384, ENSG00000160014, ENSG00000143153, ENSG00000117632, ENSG00000150625, ENSG00000128656, ENSG00000112306, ENSG00000131711, ENSG00000233927, ENSG00000184009, ENSG00000124172, ENSG00000143947, ENSG00000171617, ENSG00000162545, ENSG00000109971, ENSG00000171858, ENSG00000167526, ENSG00000108107, ENSG00000089220, ENSG00000197746, ENSG00000115268, ENSG00000137267, ENSG00000067715, ENSG00000212907, ENSG00000145592, ENSG00000088986, ENSG00000154096, ENSG00000150991, ENSG00000142937, ENSG00000147403, ENSG00000102109, ENSG00000107317, ENSG00000138326, ENSG00000172757, ENSG00000164587, ENSG00000115310, ENSG00000110436, ENSG00000130255, ENSG00000156482, ENSG00000135940, ENSG00000170027, ENSG00000167552, ENSG00000133112, ENSG00000164924, ENSG00000169567, ENSG00000111669, ENSG00000067225, ENSG00000109472, ENSG00000177954, ENSG00000177600, ENSG00000197728, ENSG00000260032, ENSG00000108298, ENSG00000071082, ENSG00000127184, ENSG00000145425, ENSG00000277586, ENSG00000149806, ENSG00000010404, ENSG00000142192, ENSG00000142541, ENSG00000186468, ENSG00000251562, ENSG00000128989, ENSG00000173915, ENSG00000092964, ENSG00000198918, ENSG00000173812, ENSG00000176788, ENSG00000122026, ENSG00000162244, ENSG00000213741, ENSG00000106976, ENSG00000167468, ENSG00000163682, ENSG00000174748, ENSG00000063177, ENSG00000148303, ENSG00000128739, ENSG00000104904, ENSG00000161016, ENSG00000113558, ENSG00000231500, ENSG00000169020, ENSG00000182899, ENSG00000014641, ENSG00000135821, ENSG00000156467, ENSG00000104888, ENSG00000166681, ENSG00000127540, ENSG00000143774, ENSG00000156298, ENSG00000110700, ENSG00000164405, ENSG00000108953, ENSG00000110955, ENSG00000172809, ENSG00000156976, ENSG00000130203, ENSG00000228253, ENSG00000131095, ENSG00000161970, ENSG00000101210, ENSG00000136854, ENSG00000171603, ENSG00000171159, ENSG00000133169, ENSG00000105640, ENSG00000171314, ENSG00000174444, ENSG00000104435, ENSG00000161203, ENSG00000105696, ENSG00000171867, ENSG00000114391, ENSG00000089009, ENSG00000142168, ENSG00000111674, ENSG00000140264, ENSG00000142676, ENSG00000102804, ENSG00000074317, ENSG00000188846, ENSG00000136942, ENSG00000109107, ENSG00000176340, ENSG00000187514, ENSG00000111716, ENSG00000156411, ENSG00000118181, ENSG00000103363, ENSG00000105372, ENSG00000198034, ENSG00000166913, ENSG00000171863, ENSG00000172020, ENSG00000220205, ENSG00000105290, ENSG00000185787, ENSG00000170906, ENSG00000196683, ENSG00000162188, ENSG00000100316, ENSG00000197958, ENSG00000184076, ENSG00000232112, ENSG00000142534, ENSG00000163536, ENSG00000133872, ENSG00000140988, ENSG00000092096, ENSG00000112695, ENSG00000168653, ENSG00000103034, ENSG00000137409, ENSG00000134419, ENSG00000127585, ENSG00000168028, ENSG00000111897, ENSG00000163399, ENSG00000172428, ENSG00000092841, ENSG00000143013, ENSG00000135916, ENSG00000198242, ENSG00000050165, ENSG00000104964, ENSG00000126432, ENSG00000106153, ENSG00000115306, ENSG00000173660, ENSG00000090266, ENSG00000074800, ENSG00000099624, ENSG00000126214, ENSG00000125462, ENSG00000126267, ENSG00000188191, ENSG00000105409, ENSG00000189241, ENSG00000109846, ENSG00000243449, ENSG00000046653, ENSG00000140319, ENSG00000102003, ENSG00000221983, ENSG00000137726, ENSG00000137154, ENSG00000131469, ENSG00000020129, ENSG00000196531, ENSG00000131507, ENSG00000147604, ENSG00000165795, ENSG00000183648
ST-DATA	ENSG00000149273, ENSG00000254709, ENSG00000137818, ENSG00000160180, ENSG00000231500, ENSG00000111640, ENSG00000034510, ENSG00000177600, ENSG00000164587, ENSG00000197756, ENSG00000105372, ENSG00000108107, ENSG00000171345, ENSG00000161016, ENSG00000167526, ENSG00000108298, ENSG00000075624, ENSG00000130255, ENSG00000105640, ENSG00000136942, ENSG00000063177, ENSG00000140988, ENSG00000112306, ENSG00000171858, ENSG00000204628, ENSG00000142541, ENSG00000117984, ENSG00000087086, ENSG00000108518, ENSG00000111341, ENSG00000115268, ENSG00000251357+ENSG00000240972, ENSG00000142534, ENSG00000105193, ENSG00000234745, ENSG00000221983, ENSG00000109062, ENSG00000182774, ENSG00000197746, ENSG00000089157, ENSG00000140264, ENSG00000177954, ENSG00000142937, ENSG00000166441, ENSG00000185499, ENSG00000246705, ENSG00000233927, ENSG00000147403, ENSG00000179218, ENSG00000213741, ENSG00000172809, ENSG00000142676, ENSG00000185624, ENSG00000137154, ENSG00000101439, ENSG00000167996, ENSG00000198034, ENSG00000257341+ENSG00000213145, ENSG00000180879, ENSG00000156482, ENSG00000141736, ENSG00000130203, ENSG00000160862, ENSG00000100316, ENSG00000164919, ENSG00000255823, ENSG00000204525, ENSG00000149806, ENSG00000269028, ENSG00000170889, ENSG00000167658, ENSG00000166710, ENSG00000083845, ENSG00000197958, ENSG00000184009, ENSG00000143947, ENSG00000145592, ENSG00000125691, ENSG00000206503, ENSG00000071082, ENSG00000162244, ENSG00000148303, ENSG00000165949, ENSG00000070756, ENSG00000019582, ENSG00000167995, ENSG00000144713, ENSG00000169710, ENSG00000163220, ENSG00000167468, ENSG00000174748, ENSG00000131469, ENSG00000152082, ENSG00000198242, ENSG00000106211, ENSG00000251562, ENSG00000138326, ENSG00000254772+ENSG00000255508, ENSG00000108821, ENSG00000279483, ENSG00000224389, ENSG00000111057, ENSG00000172757, ENSG00000110651, ENSG00000149925, ENSG00000182899, ENSG00000108639, ENSG00000172531, ENSG00000204592, ENSG00000185885+ENSG00000185201, ENSG00000149591, ENSG00000185883+ENSG00000260272, ENSG00000243678+ENSG00000011052, ENSG00000163682, ENSG00000135404, ENSG00000145425, ENSG00000108679, ENSG00000115457, ENSG00000130303, ENSG00000133112, ENSG00000273259+ENSG00000196136, ENSG00000107223, ENSG00000118181, ENSG00000124614+ENSG00000270800, ENSG00000117410, ENSG00000231925, ENSG00000178719, ENSG00000100219, ENSG00000163191, ENSG00000144426, ENSG00000106624, ENSG00000110092, ENSG00000272196, ENSG00000104904, ENSG00000188846, ENSG00000158710, ENSG00000115414, ENSG00000125534, ENSG00000185825, ENSG00000142089, ENSG00000117450, ENSG00000182492, ENSG00000087460, ENSG00000187514, ENSG00000150991, ENSG00000173272, ENSG00000169100, ENSG00000008988, ENSG00000096384, ENSG00000124614, ENSG00000092841, ENSG00000165215, ENSG00000071553, ENSG00000167815, ENSG00000114391, ENSG00000172354, ENSG00000109475, ENSG00000174444, ENSG00000160789, ENSG00000186010, ENSG00000241343+ENSG00000257529, ENSG00000204287, ENSG00000266402, ENSG00000102265, ENSG00000184897, ENSG00000186468, ENSG00000176340, ENSG00000170421, ENSG00000160932, ENSG00000074800, ENSG00000030582, ENSG00000142949, ENSG00000147604, ENSG00000170315, ENSG00000172270, ENSG00000103363, ENSG00000126267, ENSG00000205542, ENSG00000173372, ENSG00000052344, ENSG00000127540, ENSG00000122406, ENSG00000171863, ENSG00000175899, ENSG00000134419, ENSG00000026025, ENSG00000174886, ENSG00000197956, ENSG00000108344, ENSG00000196405, ENSG00000130208, ENSG00000132475, ENSG00000124172, ENSG00000196576, ENSG00000101335, ENSG00000219200+ENSG00000161939, ENSG00000123416, ENSG00000164733, ENSG00000279274, ENSG00000187608, ENSG00000196924, ENSG00000110700, ENSG00000147684, ENSG00000161960, ENSG00000277957+ENSG00000161960, ENSG00000177700, ENSG00000051523, ENSG00000182809, ENSG00000104529, ENSG00000163399, ENSG00000178952, ENSG00000163435, ENSG00000142669, ENSG00000214530, ENSG00000125730, ENSG00000143774, ENSG00000111678, ENSG00000213988, ENSG00000104964, ENSG00000058262, ENSG00000115884, ENSG00000262526+ENSG00000170296, ENSG00000105223, ENSG00000124664, ENSG00000141522, ENSG00000162511, ENSG00000126709, ENSG00000229117, ENSG00000120885, ENSG00000114353, ENSG00000123349, ENSG00000198918, ENSG00000203812, ENSG00000163479, ENSG00000131143, ENSG00000155366, ENSG00000173801, ENSG00000114867, ENSG00000089356, ENSG00000100300, ENSG00000164405, ENSG00000164692, ENSG00000198755, ENSG00000143546, ENSG00000177576+ENSG00000265681+ENSG00000215472, ENSG00000178980, ENSG00000111669, ENSG00000135390, ENSG00000159335, ENSG00000115461

Figure 3. **Genes selection in each public dataset.** This figure showcases the top 250 genes with the highest expression levels or their corresponding codes for each public dataset utilized in this task.

[4] Kristen R Maynard, Leonardo Collado-Torres, Lukas M Weber, Cedric Uytingco, Brianna K Barry, Stephen R Williams, Joseph L Catallini, Matthew N Tran, Zachary Besich, Madhavi Tippani, et al. Transcriptome-scale spatial gene expression in the human dorsolateral prefrontal cortex. *Nature neuroscience*, 24(3):425–436, 2021. 1, 4

[5] Minxing Pang, Kenong Su, and Mingyao Li. Leveraging information in spatial transcriptomics to predict super-resolution gene expression from histology images in tumors. *BioRxiv*, pages 2021–11, 2021. 2

[6] Guilherme Potje, Felipe Cadar, André Araujo, Renato Martins, and Erickson R Nascimento. Xfeat: Accelerated features for lightweight image matching. In *Proceedings of the IEEE/CVF Conference on Computer Vision and Pattern Recognition*, pages 2682–2691, 2024. 1

[7] Nicholas J Tustison, Philip A Cook, Andrew J Holbrook, Hans J Johnson, John Muschelli, Gabriel A Devenyi, Jeffrey T Duda, Sandhitsu R Das, Nicholas C Cullen, Daniel L Gillen, et al. The antsx ecosystem for quantitative biological and medical imaging. *Scientific reports*, 11(1):9068, 2021. 1

[8] Ronald Xie, Kuan Pang, Sai Chung, Catia Perciani, Sonya MacParland, Bo Wang, and Gary Bader. Spatially resolved gene expression prediction from histology images via bimodal contrastive learning. *Advances in Neural Information Processing Systems*, 36, 2024. 2

[9] Yan Yang, Md Zakir Hossain, Eric A Stone, and Shafin Rahman. Exemplar guided deep neural network for spatial transcriptomics analysis of gene expression prediction. In *Pro-*

ceedings of the IEEE/CVF Winter Conference on Applications of Computer Vision, pages 5039–5048, 2023. 2

[10] Yuansong Zeng, Zhuoyi Wei, Weijiang Yu, Rui Yin, Yuchen Yuan, Bingling Li, Zhonghui Tang, Yutong Lu, and Yuedong Yang. Spatial transcriptomics prediction from histology jointly through transformer and graph neural networks. *Briefings in Bioinformatics*, 23(5):bbac297, 2022. 2